JOURNAL OF SOLID STATE CHEMISTRY 34, 183–192 (1980)

NMR Study of Hydrogen Molybdenum Bronzes: $H_{1.71}MoO_3$ and $H_{0.36}MoO_3$

R. C. T. SLADE* AND T. K. HALSTEAD

Department of Chemistry, University of York, Heslington, York YO1 5DD, England

AND P. G. DICKENS

Inorganic Chemistry Laboratory, University of Oxford, South Parks Road, Oxford OX1 3QR, England

Received April 4, 1979; in final form August 13, 1979

Proton NMR relaxation times (T_2, T_1, and $T_{1\rho}$) and absorption spectra are reported for the compounds $H_{1.71}MoO_3$ (red monoclinic) and $H_{0.36}MoO_3$ (blue orthorhombic) in the temperature range 77 K $< T <$ 450 K. Rigid lattice dipolar spectra show that both compounds contain proton pairs, as OH_2 groups coordinated to Mo atoms in $H_{1.71}MoO_3$ and as pairs of OH groups in $H_{0.36}MoO_3$. The room temperature lineshape for $H_{1.71}MoO_3$ shows that the average chemical shielding tensor has a total anisotropy of 20.1 ppm. The relaxation measurements confirm that hydrogen diffusion occurs and give $E_A =$ 22 kJ mole^{-1} and $\tau_C^0 \simeq 10^{-13}$ sec for $H_{1.71}MoO_3$ and $E_A = 11$ kJ mole^{-1} and $\tau_C^0 \simeq 3 \times 10^{-8}$ sec for $H_{0.36}MoO_3$.

Introduction

The hydrogen molybdenum bronzes, H_xMoO_3, are ternary oxide phases formally derived from MoO_3 by insertion of atomic hydrogen. They possess a high, metal-like, conductivity, show weak temperature-independent paramagnetism, and give no ESR signal at room or liquid helium temperatures (*1*); this shows the conduction band to be highly delocalized. Glemser and co-workers (*2, 3*) reported four bronze phases. Birtill and Dickens (*4*) have characterized these as blue orthorhombic, blue monoclinic, red monoclinic, and green monoclinic phases and have given phase limits for them. Reversible electrochemical reduction of MoO_3 occurs at room temperature in aqueous acids to give a bronze (*5*),

$$\underset{\text{colorless}}{\frac{1}{x}MoO_3} + H^+ + e^- = \underset{\text{colored}}{\frac{1}{x}H_xMoO_3},$$

and this can provide the basis of an electrochromic system (*6*). The close resemblance of the powder X-ray patterns of the bronzes (*4, 7*) to that of MoO_3 and a single-crystal X-ray study of "$H_{0.5}MoO_3$" (*8*) show that insertion of hydrogen causes little crystallographic rearrangement.

Information concerning the hydrogen atom positions in the hydrogen molybdenum bronzes has come from powder neutron diffraction and inelastic neutron scattering studies (*1, 9*). Complete structure deter-

* To whom correspondence should be sent. Current address: Inorganic Chemistry Laboratory, University of Oxford, South Parks Road, Oxford OX1 3QR, England.

0022-4596/80/110183-10$02.00/0

mination of the lowest hydrogen-content, blue orthorhombic, phase has been achieved. The structure is illustrated in Fig. 1. The hydrogen atoms in this phase are located within the MoO_3 layers and attached as hydroxyl groups to bridging oxygen atoms. The neutron inelastic scattering spectrum for this phase is analogous to that for the hydrogen tungsten bronzes (*10*), H_xWO_3, both compounds being more properly formulated as nonstoichiometric oxide hydroxides, $MO_{3-x}(OH)_x$. The hydrogen positions in the higher hydrogen-content phases are not known, but the neutron inelastic scattering spectra are interpreted in terms of OH_2 groups coordinated to Mo atoms. These groups are probably in terminal positions at the top or bottom of the MoO_3 layers with the hydrogens directed toward an adjoining layer.

The proton mobility in the similar hydrogen tungsten bronzes has been studied by Vannice *et al.* (*11*), Dickens *et al.* (*12*), and Nishimura (*13*) with seemingly contradictory results. The results of neutron scattering studies (*10*) are consistent with the NMR interpretation of Dickens *et al.* but not with that of Vannice *et al.* The differences could be due to different sample preparation techniques; Dickens *et al.* worked with pure polycrystalline material whereas the other workers used powders of high surface area and susceptible to contamination by water. Nishimura's data give a diffusion coefficient for hydrogen comparable to that deduced from bleaching current measurements on electrochromic films, which are known to contain some H_2O (*14*).

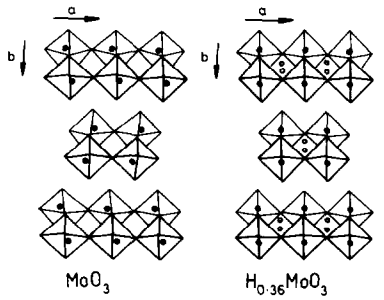

FIG. 1. The structures of MoO_3 and $H_{0.36}MoO_3$. These are represented in terms of edge- and corner-shared MoO_6 octahedra. Molybdenum atoms are represented by filled circles and hydrogen sites by open circles.

Little NMR work has been reported for the hydrogen molybdenum bronzes, but Cirillo and Fripiat (*15*) have recently reported studies of a compound $H_{1.6}MoO_3$ prepared by the hydrogen spillover method. No characterization of the material is reported, but the red monoclinic phase is produced by this method (*4*) and the reported composition is in agreement with this. Their study was primarily concerned with measurements of the spin-lattice relaxation time, T_1, in the temperature range $160\,K < T < 320\,K$ from which they deduced an activation energy for diffusion of about $30\,kJ\,mole^{-1}$. They speculate on the presence of H_2^+ ions, but this is inconsistent with neutron scattering studies (*9*) which, as discussed earlier, suggest that OH_2 groups are present. There are some brief reports of work on samples of the blue orthorhombic phase. Schoellhorn *et al.* (*5*) report a narrow absorption spectrum (1.1 G wide) at room temperature, suggesting line narrowing for "$H_{0.5}MoO_3$," and Schroeder and Weitzel (*1*) report difficulty in obtaining NMR spectra for $H_{0.31}MoO_3$, a measurable intensity being obtained only at low temperatures. In the present work, the ^1H NMR relaxation times T_2, T_1, and $T_{1\rho}$ of pure compounds $H_{1.71}MoO_3$ (red monoclinic) and $H_{0.36}MoO_3$ (blue orthorhombic) have been measured in the temperature range $77\,K < T < 450\,K$. Complementary absorption spectra have also been recorded.

Materials

Powder samples of H_xMoO_3 ($x = 1.71$, 0.36) were prepared following Glemser and co-workers (*2, 3*). All operations were carried out in an inert atmosphere.

Samples were characterized by chemical analysis and X-ray diffraction. Thermogravimetric dehydration and oxidation were followed on a Cahn RG electrobalance. The chemical reducing powder of each H_xMoO_3 sample was determined by the method of Choain and Marion (*16*). The very close agreement of the results of these analyses showed the absence of water. Powder X-ray patterns were recorded using a Debye–Scherrer camera and CuK_α radiation, the samples being mounted in Lindeman tubes to avoid oxidation. NMR samples (ca. 1 cm^3) were loaded in a dry inert atmosphere and sealed under vacuum.

Red monoclinic H_xMoO_3 was prepared by reduction of MoO_3 (Analar) with zinc and hydrochloric acid. The MoO_3 was reduced to the green phase ($x = 2.0$) and the red phase was prepared from this by dehydrogenation *in vacuo* at 383 K for 12 hr. Thermogravimetry and chemical analysis gave $x = 1.71 \pm 0.02$. The X-ray powder pattern confirmed the presence of a single monoclinic phase with $a = 13.798 \pm 0.008$Å, $b = 3.774 \pm 0.002$ Å, $c = 4.051 \pm 0.002$ Å, $\beta = 94.20°$ and is consistent with that obtained by Birtill and Dickens (*4*).

Blue orthorhombic H_xMoO_3 was prepared from MoO_3, Mo metal (Koch–Light), and distilled water, which were heated together in a sealed tube at 383 K for a month, with regular shaking. Three such preparations were attempted, only one giving a pure orthorhombic phase. Analysis gave $x = 0.36$ for the phase. The X-ray powder pattern was consistent with those of Kihlborg *et al.*(*7*) and Birtill and Dickens (*4*) and gave $a = 3.891 \pm 0.001$, $b = 14.084 \pm 0.004$, and $c = 3.738 \pm 0.001$ Å.

NMR Methods

Relaxation Time Measurements

The ^1H relaxation times of $H_{1.71}MoO_3$ and $H_{0.36}MoO_3$ were measured in the temperature range $77\,K < T < 450\,K$ using a modified Polaron spin-echo spectrometer (operating at $\omega_0/2\pi = 16$ MHz) and a Varian Fieldial magnet. The spectrometer is described in detail elsewhere (*12*). The signal-to-noise ratio was improved by routine use of a Datalab DL905 transient recorder interfaced with a Datalab DL102 averager.

The spin-lattice relaxation time, T_1, of $H_{1.71}MoO_3$ was measured using a 90°–τ–90° pulse sequence. To prevent saturation effects, the repeat time between successive cycles was kept $>6T_1$ for this compund. The signal-to-noise ratio for observed decays for $H_{0.36}MoO_3$ was very poor and averaging was necessary to see any decay at all. T_1 for this compound was therefore measured using a multiple-pulse saturation method, $90°–(\tau–90°)_n$, and T_1 was determined from the steady state amplitude, $M(\tau)$, of the free induction decay (FID) using the formula (*17*)

$$M(\tau) = M(\infty)\,(1 - \exp(-\tau/T_1)).$$

This latter method gives very considerable time savings in measurement of long T_1's for compounds giving very weak signals, for which hundreds of sequences need to be accumulated. Values determined by the 90°–τ–90° method agreed within experimental uncertainty.

$T_{1\rho}$, the spin-lattice relaxation time in the rotating frame, was measured using the method of Hartmann and Hahn (*18*). The B_1 field strength, determined from the length of a 90° pulse, was 8 G.

In the motionally narrowed regions, T_2, the spin–spin relaxation time, was measured from the FID or by the Carr–Purcell–Meiboom–Gill pulse sequence (*19*). At lower temperatures (in the rigid lattice regions), T_2 was measured using the zero-time-resolution (ZTR) technique (*20*), T_2 being taken as the time for the solid echo to decay to $1/e$ of its maximum height, as is done conventionally. The second moment, M_2, was calculated using the ZTR technique from the curvature of the solid echo at its maximum (*21*).

Absorption Signal Measurements

Continuous wave (CW) broad-line spectra were recorded at a temperature of 100 K using a Varian WL-112 spectrometer operating at $\omega_0/2\pi = 15$ MHz. The samples used were $H_{1.68}MoO_3$ and $H_{0.34}MoO_3$ prepared by Birtill and Dickens (*4*).

Absorption spectra of $H_{1.71}MoO_3$ and $H_{0.36}MoO_3$ at room temperature and 130 K were obtained by Fourier transformation of FIDs using a Bruker CXP spectrometer operating at $\omega_0/2\pi = 90$ MHz. Rigid lattice dipolar spectra are slightly distorted by uncertainties in the time zero but narrower lines are negligibly affected. Spectra produced using the ZTR technique (*20*) do not suffer from this but are distorted by dipolar error terms.

Results

Absorption Spectra and Second Moments

The CW absorption spectra recorded at 100 K had poor signal-to-noise ratios but it was possible to estimate second-moment (M_2) values (corrected for modulation broadening) of 25 G^2 for $H_{1.68}MoO_3$ and 5 G^2 for $H_{0.34}MoO_3$. The derivative signals for both compounds showed two components, a narrow central signal and a broader one, but further details were lost in noise and modulation effects. M_2 values for $H_{1.71}MoO_3$ and $H_{0.36}MoO_3$ calculated using the ZTR technique were 23 ± 1 and 5.7 ± 0.4 G^2, respectively.

Figure 2 shows the absorption spectra obtained by Fourier transformation for $H_{1.71}MoO_3$. The room temperature line is very narrow (about 2 kHz wide) and asymmetrical. The low-temperature (rigid lattice) lineshape is consistent with the CW spectrum. The separation of the shoulders (or side peaks) is about 11 G.

Figure 3 shows the low-temperature (rigid lattice) lineshape obtained by Fourier transformation for $H_{0.36}MoO_3$ and is consistent

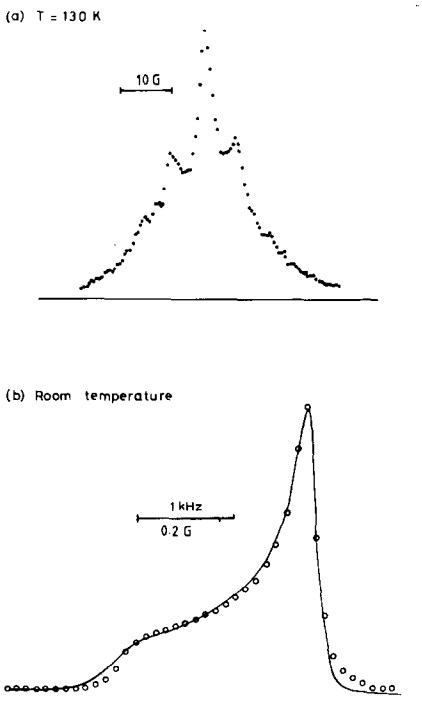

FIG. 2. Absorption spectra of $H_{1.71}MoO_3$ produced by Fourier transformation. (a) 130 K: the rigid lattice dipolar spectrum. (b) Room temperature: a motionally narrowed spectrum showing an axially symmetric anisotropic chemical shielding tensor. The solid line is the experimental lineshape. The open circles show the least-squares fit to the theoretical lineshape (total anisotropy $\Delta\sigma = 20.1$ ppm) convoluted with a Lorentzian broadening function (half-width $w = 108$ *Hz*).

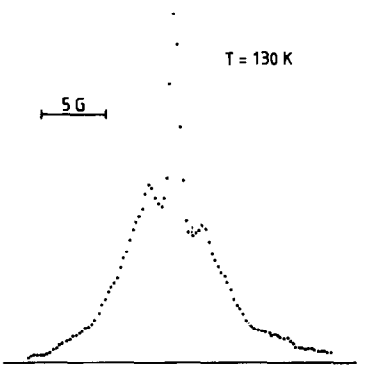

FIG. 3. The rigid lattice dipolar spectrum of $H_{0.36}MoO_3$ produced by Fourier transformation.

with the CW spectrum. The separation of the side peaks is 4.1 G. The room temperature spectrum is asymmetric and shows some line narrowing.

Relaxation times

Figure 4 shows the temperature dependence of the relaxation times T_2, T_1, and $T_{1\rho}$ for $H_{1.71}MoO_3$. Data were analyzed using least-squares fitting procedures. At temperatures below 160 K spin-lattice relaxation was nonexponential and T_1 was defined to be the time for $(M(\infty)-M(\tau))$ to decay to $1/e$ of its initial value.

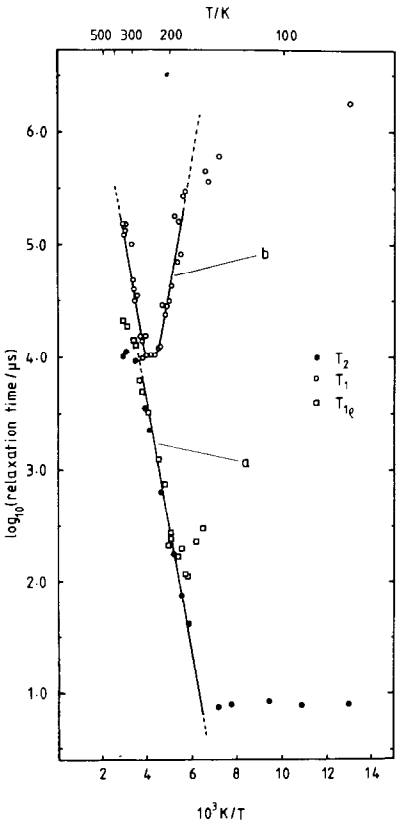

FIG. 4. Temperature dependence of relaxation times for $H_{1.71}MoO_3$. At high temperatures T_2, T_1, and $T_{1\rho}$ are determined by modulation of the dipolar interaction by diffusion of hydrogen. (a) The solid line is the high-temperature behavior of T_2 and $T_{1\rho}$ calculated with $E_A = 22$ kJ mole^{-1}. (b) The solid line shows the least-squares fit (with $E_A = 22.1$ kJ mole^{-1} and $\tau_c^0 = 8.8 \times 10^{-14}$ sec) of the T_1 data to BPP theory.

Figure 5 shows the temperature dependence of T_2 for $H_{0.36}MoO_3$. Spin-lattice relaxation in both the laboratory and rotating frames was always nonexponential, T_1 then being defined as in the previous paragraph and $T_{1\rho}$ as the length of the spin-locking pulse which reduced the amplitude of the subsequent FID to $1/e$ of its initial value. This nonexponentiality, together with the extremely poor signal-to-noise ratio for this compound, led to a large scatter in T_1 and $T_{1\rho}$ values, which were only slightly temperature dependent. T_1 values were in the range 100–400 msec and $T_{1\rho}$ values in the range 0.4–1.8 msec.

Discussion

1. Relaxation Behavior

Red monoclinic $H_{1.71}MoO_3$. Motional narrowing occurs at $T > 150$ K and T_1, T_2, and $T_{1\rho}$ are all very similar at room temperature, showing there is rapid diffusion of hydrogen. A random walk model would require information about hydrogen positions, which is currently not available. The

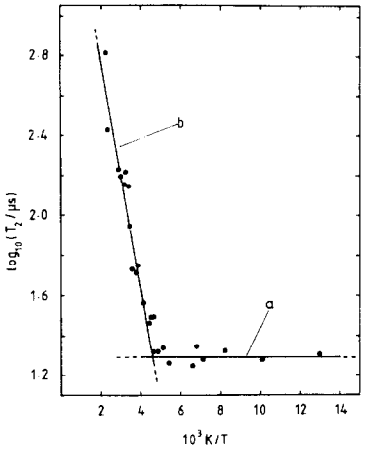

FIG. 5. Temperature dependence of T_2 for $H_{0.36}MoO_3$ (a) T_2 is determined by "rigid" dipolar interactions. The solid line was calculated using the formula $T_2 = (2\gamma^2 M_2/\pi)^{-1/2}$. (b) T_2 is determined by modulation of the dipolar interaction by hydrogen diffusion. The solid line is the least-squares fit to BPP theory (with $E_A = 11.0$ kJ mole^{-1}, $\tau_c^0 = 2.9 \times 10^{-8}$ sec).

well-known BPP model (*22*), which ignores the lattice but is a good approximation in many cases, was therefore used. In the line narrowing region $T_2 \propto \tau_c^{-1}$, where τ_c is the correlation time (mean time for which the dipolar coupling is unchanged). The temperature dependence of T_2 (and hence of τ_c) has an Arrhenius form with $E_A = 21.9 \pm 0.3$ kJ mole^{-1} in this region. Similarly $T_{1\rho} \propto \tau_c^{-1}$ at temperatures above the $T_{1\rho}$ minimum and the data give $E_A = 21.8 \pm 1.4$ kJ mole^{-1}. Least-squares fitting of the T_1 minimum gives $E_A = 22.1 \pm 1.5$ kJ mole^{-1} and $\tau_c^0 = (8.8 \pm 6.5) \times 10^{-14}$ sec. The close agreement of these figures shows that no distribution of sites or correlation times need be considered.

The T_1 minimum predicted from the low-temperature M_2 value (23 G^2) is $\simeq$7 msec. The experimental value is 10.1 ± 0.6 msec. This discrepancy is not understood.

A minimum in $T_{1\rho}$ occurs at $\simeq$110 μsec, measurements currently being difficult due to loss of most of the decay in the instrument dead time. For the fields used in this work, the ratio $(T_1)_{min} : (T_{1\rho})_{min}$ expected from BPP theory is 120:1. The experimental value is 90:1. BPP theory is valid in the weak collision limit, i.e., when $B_L' \ll B_1$, where $B_L' = (\frac{1}{3}M_2)^{1/2}$ and is the local dipolar field in the rotating frame. In this case $B_L' = 2.8$ G, which is not small compared with B_1. Weak collision theories are therefore not entirely valid for $T_{1\rho}$, but we know of no other suitable theory.

T_2 shows a high-temperature plateau ($\simeq$10 msec, see Fig. 4). Cirillo and Fripiat (*15*) also observed a plateau ($\simeq$3 msec) in their measurements on $H_{1.64}MoO_3$ by the spin–echo technique and ascribed it to field inhomogeneities arising from the bulk magnetization of the particles. However, both the CPMG and spin-echo techniques remove the effects of static inhomogeneities and chemical shielding anisotropies. The occurrence of the plateau is not understood but shows that some residual interaction has not been removed by the pulse sequence or by hydrogen diffusion. One possibility is that diffusion is anisotropic or relatively short range, thus leading to a residual dipolar interaction. Another is that some interaction having a correlation time much shorter than the period between the CPMG pulses is not removed.

At low temperatures ($T < 160$ K), T_1 deviates from the values predicted if motional modulation of the dipolar inter-proton interaction were the only relaxation mechanism. The temperature dependence of T_1 is then only slight and the relaxation is nonexponential. This results from relaxation via paramagnetic (impurity) centers. The temperature dependence is that of T_1^e (the relaxation time of the centers) and it follows from the temperature at which T_1 becomes only slightly temperature dependent that $T_1^e < 10^{-6}$ sec (*23*). At low temperature, θ (the time for hydrogens to diffuse between impurities, ca. $100\,\tau_c$) becomes long compared with T_1 and spatial averaging of relaxation rates is no longer performed. Relaxation then occurs at different rates for ions close to and far from the centers and is consequently nonexponential. The paramagnetic species are not Mo atoms because the electrons donated on reduction of MoO_3 go into the conduction band and do not give localized Mo(VI–x) species.

The results for $H_{1.71}MoO_3$ can be compared with those of Cirillo and Fripiat (*15*). Their analysis of T_1 data is in terms of Torrey's theory of isotropic diffusion (*24*) and is mostly in the limit where the flight path is long and where the equations are as in the BPP theory used here. They obtain $E_A = 30$ kJ mole^{-1}, whereas here we obtain $E_A = 22$ kJ mole^{-1}. The difference in values could simply reflect the higher hydrogen content of the material used in this work. Cirillo and Fripiat include relaxation via conduction electrons as an important relaxation process. It is not found necessary to consider this

mechanism in interpreting measurements at 16 MHz.

Blue orthorhombic $H_{0.36}MoO_3$. Motional narrowing occurs at $T > 215$ K (see Fig. 5). It follows from BPP theory that $T_2 \propto \tau_c^{-1}$ in the line narrowing region and the Arrhenius behavior gives $E_A = 11.0 \pm 1.1$ kJ mole^{-1} and $\tau_c^0 = (3.2 \pm 1.3) \times 10^{-8}$ sec. The poor signal-to-noise ratio is due to both the low hydrogen content and the high electronic conductivity, which prevents the RF from penetrating far into the powder particles.

The weak temperature dependence of T_1 and $T_{1\rho}$ shows that motional modulation of dipolar interactions is not the dominant relaxation process. Attempts were made to analyze the nonexponential relaxation in terms of two exponentials, but this is arbitrary and there were wide variations in the amplitudes of the two exponentials. The behavior is analogous to that of $H_{1.71}MoO_3$ at low temperatures which was interpreted in terms of paramagnetic (impurity) centers.

2. *Dipolar Spectra*

Red monoclinic $H_{1.71}MoO_3$. The NMR lineshape at 130 K (Fig. 2a) is not the simple Pake doublet (*25*) that would be expected if all the hydrogens were present in OH_2 groups (see introduction). The separation of the side peaks is similar to the doublet splitting for gypsum ($CaSO_4 \cdot 2H_2O$) and these are attributable to those hydrogens which are in OH_2 groups. The central peak arises from the remaining hydrogens, which are presumably present as hydroxyl groups. Estimation of the areas under the absorption curve due to these two hydrogen environments suggests that $\simeq$90% of the hydrogens are present in OH_2 groups.

Blue orthorhombic $H_{0.36}MoO_3$. The hydrogen atom sites in this phase are known to be within the MoO_3 layers and in a zig-zag chain of oxygen atoms, this being illustrated in Fig. 6a. The stoichiometry $H_{0.36}MoO_3$ corresponds to an average occupancy of 0.18 for these sites. Two sites on a given O . . . O line

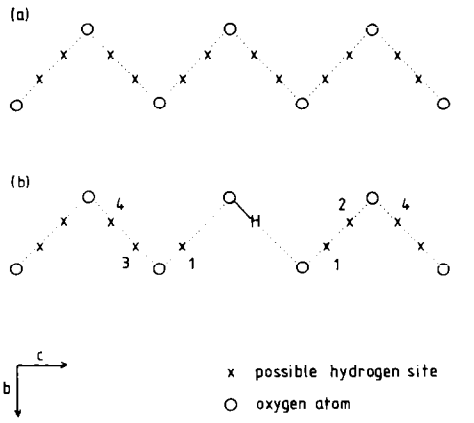

FIG. 6. The intralayer zigzag of oxygen atoms in $H_{0.36}MoO_3$. (a) The average structure (hydrogen site occupancy = 0.18). (b) The available sites near an occupied site (hydroxyl group).

are too close for simultaneous occupation and neutron inelastic scattering detected no OH_2 groups in this phase (*9*). The sites which may be occupied near an occupied site (hydroxyl group) are shown in Fig. 6b. The distances of these from the hydroxyl hydrogen are 2.02 Å for type 1, 2.40 Å for type 2, 3.39 Å for type 3, and 3.74 Å for type 4, these values being calculated from the atom coordinates given by Dickens *et al.* (*9*).

The experimental M_2 value for $H_{0.36}MoO_3$ is $\simeq 5$ G^2. Contributions to M_2 from interactions with Mo atoms and with hydrogens in different chains are negligible. For the hydroxyl hydrogen in Fig. 6b, the M_2 contributions (in the van Vleck formula) from interactions with hydrogens on other sites would be 5.3 G^2 for a type 1 site, 2.4 G^2 for a type 2, 0.24 G^2 for a type 3, and 0.13 G^2 for a type 4. To account for the experimental M_2, most ($\simeq$90%) of the hydrogens must have a neighboring type 1 site occupied. This does not correspond to a random distribution but suggests that most of the hydrogens are in pairs, the chance of three hydrogens close together being small.

The lineshape for $H_{0.36}MoO_3$ (Fig. 3) is similar to that for $H_{1.71}MoO_3$ but consider-

ably narrower. The side peaks arise from pairs of protons of the type discussed in the previous paragraph. To a first approximation, the side peak separation, ΔB, is related to the intrapair separation, R, by (*25*) $\Delta B = \frac{3}{2}\gamma\hbar(\mu_0/4\pi)R^{-3}$. The observed $\Delta B = 4.1$ G corresponds to $R \simeq 2.2$ Å, which is close to the separation (2.02 Å) predicted from the model above. The central peak arises from those hydrogens not in pairs of hydroxyl groups and estimation of the areas under the absorption curve due to these two environments shows that ≃90% of the hydroxyl groups are paired, in good agreement with the conclusions of the previous paragraph.

3. *Chemical Shielding*

Red monoclinic $H_{1.71}MoO_3$. The room temperature lineshape observed for $H_{1.71}MoO_3$ (Fig. 2b) can be most readily explained as arising from an axially symmetric chemical shielding tensor in a powder sample where the dipolar interaction has been largely removed. A total anisotropy $\Delta\sigma = 20.1$ ppm was calculated using a least-squares fit to the theoretical lineshape (*26*) convoluted with a Lorentzian broadening function (representing the residual dipolar interactions) of half-width w. The residual dipolar interaction also determines T_2^{CPMG} because the CPMG pulse sequence removes the interaction due to anisotropic shielding, which motion does not remove. Since for a Lorentzian line $T_2 = 1/w$, the experimental $T_2^{CPMG} = 9.3$ msec and the fitted $w = 108$ Hz are consistent.

Spectra similar to that in Fig. 2b were reported by Cirillo and Fripiat (*15*), who assign the lineshape to an unspecified anisotropic magnetic broadening. Figure 7 shows calculated lineshapes for a range of values of $10^6 w/(\Delta\sigma\nu_0)$. If the dipolar interaction is modulated by atomic diffusion, w, and hence also $10^6 w/(\Delta\sigma\nu_0)$, decreases with increasing temperature at a given Larmor frequency, ν_0. These spectra are very similar to those in Figs. 1–3 of Cirillo and Fripiat's work. From our data we calculate $10^6 w/(\Delta\sigma\nu_0) = 0.3$ at about 200 K for measurements at 90 MHz.

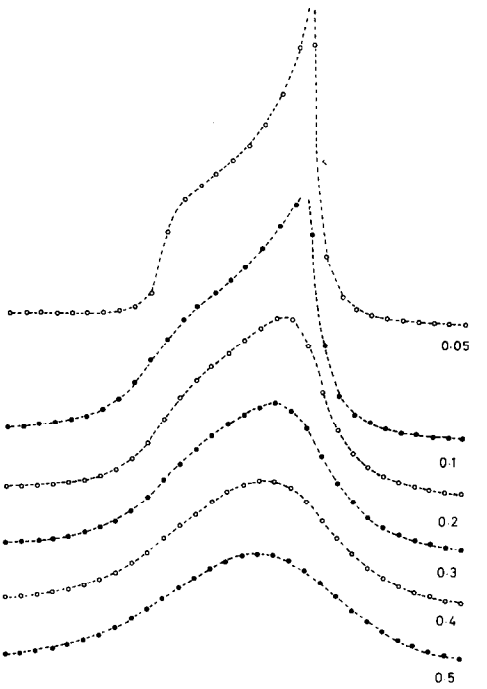

FIG. 7. The effect on absorption lineshape of chemical shielding anisotropy and dipolar broadening. Computed lineshapes arising from an axially symmetric anisotropic chemical shielding tensor (total anisotropy $\Delta\sigma$) and Lorentzian broadening (half-width w) for a range of values of $10^6 w/(\Delta\sigma\nu_0)$. The area under each absorption curve is the same.

The observed chemical shielding anisotropy is an average brought about by diffusion of hydrogen nuclei, this process largely removing the (homo- and heteronuclear) dipolar interaction. For periods less than 10 msec the mean square displacement of hydrogen nuclei is much less than the particle size estimated from specific surface area measurements ($3.7\ m^2\ g^{-1}$). Therefore in interpreting NMR lineshapes we have assumed that a given hydrogen nucleus is confined to a single particle. The shielding tensor, $\boldsymbol{\sigma}^i$, is in principle different (i.e., there is an NMR line) for each magnetically

inequivalent site in a particle and the powder spectrum is the superposition of all the NMR lines from all the randomly oriented particles. As the hydrogen nuclei diffuse from one site to another, only the time-average shielding tensor is observable and this is determined by the space-average (i.e., average over all the sites in a particle) chemical shielding tensor, $\bar{\boldsymbol{\sigma}}^s$. $H_{1.71}MoO_3$ is monoclinic and one principal axis of the site-average tensor is required by symmetry to lie parallel to the *b*-axis. Furthermore the hydrogen positions in $H_{1.71}MoO_3$ must be such that $\bar{\boldsymbol{\sigma}}^s$ is axially symmetric with the unique shielding direction corresponding to the least-shielded direction, as observed experimentally.

The diffusion of hydrogen nuclei, which gives the site-average tensor, $\bar{\boldsymbol{\sigma}}^s$, is likely to be between sites located in hydrogen bonds. According to Haeberlen (*27*), the chemical shielding tensor of H in H bonds, $\boldsymbol{\sigma}^{\text{H bond}}$, is determined predominantly by the electron distribution within the bond. Usually $\boldsymbol{\sigma}^{\text{H bond}}$ is approximately axially symmetric with the unique shielding direction lying nearly along the axis of the bond. Typical total anisotropies $\Delta\sigma^{\text{H bond}}$) are 20 ppm for $MgSO_4 \cdot H_2O$ and 37 ppm for KH_2PO_4 (*27*). The observed total anisotropy (20 ppm) is therefore reasonable for a site-average tensor.

Chemical shielding tensors are usually determined using multiple-pulse sequences or magic angle spinning, but here we have taken advantage of atomic diffusion to determine the site-average tensor.

4. *Diffusion*

The parameters $E_A \simeq 20\ \text{kJ mole}^{-1}$ and $\tau_c^0 \simeq 10^{-13}$ sec are typical of materials showing fast hydrogen diffusion. This is true, for instance, of the compounds $H_{1.71}MoO_3$ (this work), $HUO_2PO_4 \cdot 4H_2O$ (*28*), and $LaNi_5H_6$ (*29*). Molecular/bond vibration frequencies are typically 1000–3000 cm^{-1} (i.e., $\simeq 10^{13}$ Hz). Hence $(\tau_c^0)^{-1}$ may be interpreted as a bond vibration frequency.

The motional parameters for hydrogen diffusion in $H_{0.36}MoO_3$ ($E_A = 11\ \text{kJ mole}^{-1}$ and $\tau_c^0 \simeq 3 \times 10^{-8}$ sec) are very similar to those found for $H_{0.46}WO_3$ ($E_A = 16\ \text{kJ mole}^{-1}$ and $\tau_c^0 = 7 \times 10^{-8}$ sec) by Dickens *et al.* (*12*). Both compounds are nonstoichiometric oxide hydroxides.

Self-diffusion coefficients and associated ionic conductivities for the hydrogens in $H_{1.71}MoO_3$ and $H_{0.36}MoO_3$ can be estimated using random walk theory (see, e.g., Ref. (*30*)). The mean time between jumps, τ_d, is twice the dipolar field correlation time, τ_c, as the field changes whenever either of a pair of proton jumps. Diffusion in $H_{1.71}MoO_3$ involves jumping along an O . . . O line. The jump distance would be about 1 Å and hence $D_0 \simeq 10^{-4}\ \text{cm}^2\ \text{sec}^{-1}$ and $D(300\ \text{K}) \simeq 10^{-8}\ \text{cm}^2\ \text{sec}^{-1}$. In $H_{0.36}MoO_3$ a possible diffusion path is along the zigzag chain of oxygens within a layer, the jump distance again being about 1 Å, and this gives $D_0 \simeq 10^{-9}\ \text{cm}^2\ \text{sec}^{-1}$ and $D(300\ \text{K}) \simeq 10^{-11}\ \text{cm}^2\ \text{sec}^{-1}$. Ionic conductivities can be estimated using the Nernst–Einstein relationship, assuming a Haven ratio of unity and no enhancement due to electron–ion coupling. This gives $\sigma(300\ \text{K}) \simeq 2 \times 10^{-3}\ \text{ohm}^{-1}\ \text{cm}^{-1}$ for $H_{1.71}MoO_3$, which would qualify it as a superionic conductor (*30*). The corresponding figure for $H_{0.36}MoO_3$ is $\sigma(399\ \text{K}) \simeq 4 \times 10^{-7}\ \text{ohm}^{-1}\ \text{cm}^{-1}$, showing this material to have only a poor ionic conductivity.

Acknowledgment

We thank Dr. B. C. Silbernagel of Exxon Research and Engineering Company for help with broad-line absorption spectra. We thank Bruker-Physik AG for use of equipment at their Applications Laboratory. We thank the Science Research Council for a Fellowship for R.C.T.S.

References

1. F. A. SCHROEDER AND H. WEITZEL, *Z. Anorg. Allg. Chem.* **435**, 247 (1977).

2. O. GLEMSER AND G. LUTZ, *Z. Anorg. Allg. Chem.* **264**, 17 (1951).
3. O. GLEMSER, G. LUTZ, AND G. MEYER, *Z. Anorg. Allg. Chem.* **285**, 173 (1956).
4. J. J. BIRTILL AND P. G. DICKENS, *Mater. Res. Bull.* **13**, 311 (1978).
5. R. SCHOELLHORN, R. KUHLMANN, AND J. O. BESENHARD, *Mater. Res. Bull.* **11**, 83 (1976).
6. I. F. CHANG, B. L. GILBERT, AND T. I. SUN, *J. Electrochem. Soc.* **122**, 955 (1975).
7. L. KIHLBORG, G. HAGERSTROM, AND A. RONNQUIST, *Acta Chem. Scand.* **15**, 1187 (1961).
8. K. A. WILHELMI, *Acta Chem. Scand.* **23**, 419 (1969).
9. P. G. DICKENS, J. J. BIRTILL, AND C. J. WRIGHT, *J. Solid State Chem.* **28**, 185 (1979).
10. C. J. WRIGHT, *J. Solid State Chem.* **20**, 89 (1977).
11. M. A. VANNICE, M. BOUDART, AND J. J. FRIPIAT, *J. Catal.* **17**, 359 (1970).
12. P. G. DICKENS, D. J. MURPHY, AND T. K. HALSTEAD, *J. Solid State Chem.* **6**, 370 (1973).
13. K. NISHIMURA, *Solid State Commun.* **20**, 523 (1976).
14. R. HURDITCH, *Electron. Lett.* **11**, 142 (1975).
15. A. CIRILLO AND J. J. FRIPIAT, *J. Phys. (Paris)* **39**, 247 (1978).
16. C. CHOAIN AND F. MARION, *Bull. Soc. Chim. Fr.* 212 (1963).
17. D. C. LOOK AND D. R. LOCKER, *Rev. Sci. Instrum.* **41**, 250 (1970).
18. S. R. HARTMANN AND E. L. HAHN, *Phys. Rev.* **128**, 2047 (1962).
19. S. MEIBOOM AND D. GILL, *Rev. Sci. Instrum.* **29**, 688 (1958).
20. J. G. POWLES AND J. H. STRANGE, *Proc. Phys. Soc. London* **82**, 6 (1963).
21. P. MANSFIELD, *Phys. Rev.* **137**, A961 (1965).
22. A. ABRAGAM, "The Principles of Nuclear Magnetism," p. 462 Oxford Univ. Press, London New York (1961).
23. H. A. RESING, *Advan. Mol. Relaxation Processes* **3**, 199 (1972).
24. H. C. TORREY, *Phys. Rev.* **92**, 962 (1953).
25. A. ABRAGAM, "The Principles of Nuclear Magnetism," p. 220, Oxford Univ. Press, London/New York (1961).
26. M. MEHRING, "High Resolution N.M.R. Spectroscopy in Solids," *N.M.R. Basic Princ. Progr.* **11**, 22 (1976).
27. U. HAEBERLEN, "High Resolution N.M.R. in Solids," *Advan. Magn. Reson. Suppl. 1* (1976).
28. P. E. CHILDS, T. K. HALSTEAD, A. T. HOWE, AND M. G. SHILTON, *Mater. Res. Bull.* **13**, 609 (1978).
29. T. K. HALSTEAD, H. A. ABOOD, AND K. H. J. BUSCHOW, *Solid State Commun.* **19**, 425 (1976).
30. P. MCGEEHIN AND A. HOOPER, *J. Mater. Sci.* **21**, 1 (1977).